4

Unimolecular Dissociation of γ-Ketohydroperoxide

Hydroperoxides (molecules containing -OOH group) are important in the gas and liquid phase oxidation of organic compounds. They are also important in combustion chemistry[Wang *et al.*, 2019] due to their role in the first and second stage auto-ignition of gasoline and diesel fuel components[Saxena and Bedoya, 2013; Musculus *et al.*, 2013; Battin-Leclerc, 2008; Westbrook *et al.*, 2018]. Organic hydroperoxides play a central role in the atmospheric oxidation reactions and their degradation in troposphere results in low vapor pressure polyfunctional species that lead to the formation of secondary organic aerosols[Guo *et al.*, 2014; Docherty *et al.*, 2005]. The O-O bond in these compounds is weaker than C-C or C-H bonds and responsible for the formation of radicals[Luo, 2007]. Kinetic studies of organic hydroperoxides are limited because they are highly reactive and difficult to obtain commercially[Wang *et al.*, 2019; Kyasa *et al.*, 2013]. Due to the limitations associated with analytical techniques, the unimolecular reactivity of these molecules has been investigated by theoretical models[Pfaendtner and Broadbelt, 2008]. The molecule of interest in the present work is $\gamma-$ketohydroperoxide, [3-(hydroperoxy)propanal, $HOOCH_2CH_2CHO$, abbreviated as KHP] and it is considered to be the primary source of radicals in low temperature combustion[Zádor *et al.*, 2011]. Ketohydroperoxides have been observed in gas-phase alkane oxidation experiments along with high yields of carboxylic acids[Cord *et al.*, 2012; Battin-Leclerc *et al.*, 2011]. Qi and co-workers have provided strong experimental evidence for the presence of KHP in the low temperature oxidation of alkanes[Battin-Leclerc *et al.*, 2010]. The O-O cleavage is considered to be the primary dissociation pathway of KHP. Jalan et al.,[Jalan *et al.*, 2013] investigated the Korcek decomposition of[Jensen *et al.*, 1979] KHP to form CH_3CHO (acetaldehyde) + HCOOH (formic acid) or CH_3COOH (acetic acid) + HCHO (formaldehyde) products at the CCSD(T)//M06-2X level of electronic structure theory. Their calculations showed that the Korcek reaction of KHP is highly exoergic. The reaction mechanism involved the formation of a cyclic-peroxide intermediate which decomposed to the carbonyl and carboxylic acid products. These calculations showed that Korcek pathway is energetically favored over the O-O homolytic dissociation. Further, it was found that acid catalyzed cyclic peroxide formation reaction (in the condensed phase) had much lower potential energy barrier in comparison to the same reaction in the gas phase.

Truhlar and co-workers[Xing *et al.*, 2017] have reported theoretical studies of the kinetics of H abstraction from the related 4-hydroperoxy-2-pentanone [$HOOCH(CH_3)CH_2C(CH_3)O$] molecule by OH radical. Electronic structure theory calculations and a combination of master equation and direct classical trajectory method was used to study the thermal decomposition of KHP to four product channels including the Korcek pathway[Goldsmith *et al.*, 2015]. In this study, O-O dissociation of KHP resulting in radicals was found to be dominant above 600 K and the other molecular channels were observed below 400 K temperature. In the same work, Born-Oppenheimer direct classical trajectory method was used to study the product energy partitioning of the $HOOCH_2CH_2CHO$ + OH reaction products. The trajectories were launched from the bimolecular transition state and *on-the-fly* integrations were performed at the density functional M06-2X/6-31+G(d,p) level of theory.

Automated reaction path discovery methods[Suleimanov and Green, 2015; Maeda and Harabuchi, 2019; Grambow *et al.*, 2018] were used to study the unimolecular decomposition of KHP. Suleimanov et al.,[Suleimanov and Green, 2015] used the freezing string and Berny transition

state (TS) optimization methods to identify TSs for six unimolecular decomposition pathways of KHP which included the previously reported Korcek reaction. Harabuchi and co-workers[Maeda and Harabuchi, 2019] have used single-component artificial force induced reaction method to study the decomposition of KHP. Grambow et al.,[Grambow *et al.*, 2018] combined density functional theory with different automated transition state search algorithms and found 75 elementary unimolecular reactions of KHP and they were classified under different reaction channels. At this point, it is worth mentioning that malondialdehyde [$CH_2(CHO)_2$] and acrolein [CH_2CHCHO] channels were identified in these studies which were observed as important dissociation pathways in the study reported here. In the present work, unimolecular dissociation chemistry of KHP was investigated using electronic structure theory and Born-Oppenheimer direct chemical diynamics simulations. As mentioned above, large number of unimolecular reactions of KHP have been identified using automated reaction discovery methods. The primary objectives here are to (a) identify which pathways are actually important under gas phase reaction conditions at elevated temperatures among the possible reaction networks of KHP and (b) establish atomic level dissociation mechanisms which have not been reported earlier.

4.1 METHODOLOGY AND PES

Classical trajectories were launched from the reactant well and integrated using potentials and gradients obtained *on-the-fly* at the B3LYP/6-31+G* level of theory. The selected method is accurate enough and also computationally feasible to generate sufficient number of direct dynamics trajectories to make statistically meaningful predictions. Simulations were performed at three different total energies, E_{tot} = 200, 250, and 300 kcal/mol. These energy values were selected such that all the reaction pathways are accessible and the simulations can be completed in a reasonable amount of computational time. To select the initial conditions, the total energies were distributed among the normal mode vibrations of KHP using classical micro-canonical sampling technique[Peslherbe *et al.*, 1999; Hase and Buckowski, 1980] with no rotational energies. With an integration time-step of 0.5 fs, the trajectories were propagated to a total time of 2 ps or until dissociation products were separated by a distance of 12.0 Å. A 6th order Symplectic integrator[Schlier and Seiter, 1998, 2000] was used to perform the trajectory integrations.

Stationary points on the dissociation energy profile of KHP were characterized using different levels of electronic structure theory. Equilibrium points and TSs were energy minimized and harmonic vibrational frequencies were used to differentiate a minimum from a saddle point. Intrinsic reaction coordinate (IRC) calculations were performed to check whether a given TS connects correct product(s) with the reactant. The results are summarized in Table 4.1 which shows energies (in kcal/mol, zero point energy not corrected) of various stationary points relative to KHP. Benchmark CCSD(T) values in the table are single point energies computed using MP2 optimized geometries with the same basis set. Direct dynamics simulations are computationally expensive and by considering computational cost and accuracy, B3LYP/6-31+G* method was selected to perform the dynamics simulations. Simulation conditions were sufficient to maintain energy conservation in the trajectories within $E_{tot} \pm 1.0$ kcal/mol. E_{tot} as a function of time is shown for few trajectories in Figure 4.1.

Figure 4.2 shows the potential energy profiles for the decomposition of KHP (in kcal/mol) without zero point energy corrections computed using B3LYP/6-31+G* theory. Among the dissociation pathways of KHP predicted using automated reaction discovery methods[Grambow *et al.*, 2018], Figure 4.2 shows only those observed in the dynamics simulations in an appreciable number of trajectories. As is evident from Figure 4.2, the O-O dissociation resulting in OH + OCH_2CH_2CHO products has the largest energy requirement (64.6 kcal/mol). The Korcek decomposition has a moderate energy barrier (TS1, 34.4 kcal/mol) and is highly exoergic, consistent with previous CCSD(T)//M06-2X level calculations[Jalan *et al.*, 2013]. First step of Korcek

Table 4.1: Stationary point energies (in kcal/mol) for the unimolecular dissociation of KHP computed using different levels of theory. The given values are relative to respective KHP energies and zero point energy not corrected.

Stationary Point	B3LYP/ 6-31+G*	PBE0/ 6-31+G*	M06-2X/ 6-31+G*	MP2/ 6-31+G*	CCSD(T)// MP2/ 6-31+G*	CCSD(T)// MP2/ 6-311++G*
KHP	0.0	0.0	0.0	0.0	0.0	0.0
HO + OCH_2CH_2CHO	64.6	71.5	93.0	139.7	40.7	40.6
TS1	34.4	30.4	33.6	34.0	36.8	39.7
c-$C_3H_6O_3$[e]	-8.9	-13.8	-13.5	-10.6	-10.7	-9.7
TS2A	29.0	28.9	36.2	45.3	28.3	25.8
INT2A	-75.7	-73.4	-75.2	-79.6	-79.2	-76.7
CH_3COOH + HCHO	-67.3	-64.0	-64.9	-69.9	-66.4	-68.1
TS2B	26.0	26.0	34.0	42.7	26.8	25.2
INT2B	-78.3	-76.0	-75.8	-81.2	-77.4	-77.9
HCOOH + CH_3CHO	-69.4	-66.1	-65.9	-71.2	-67.3	-68.9
TS3	50.4	54.4	62.3	52.1	31.8	31.6
H_2O + $CH_2(CHO)_2$	-39.8	-38.7	-39.9	-43.2	-51.8	-52.0
TS4	55.0	52.1	54.2	55.2	57.6	60.1
HOOH + CH_2CHCHO	16.8	22.4	22.6	19.1	18.0	20.1

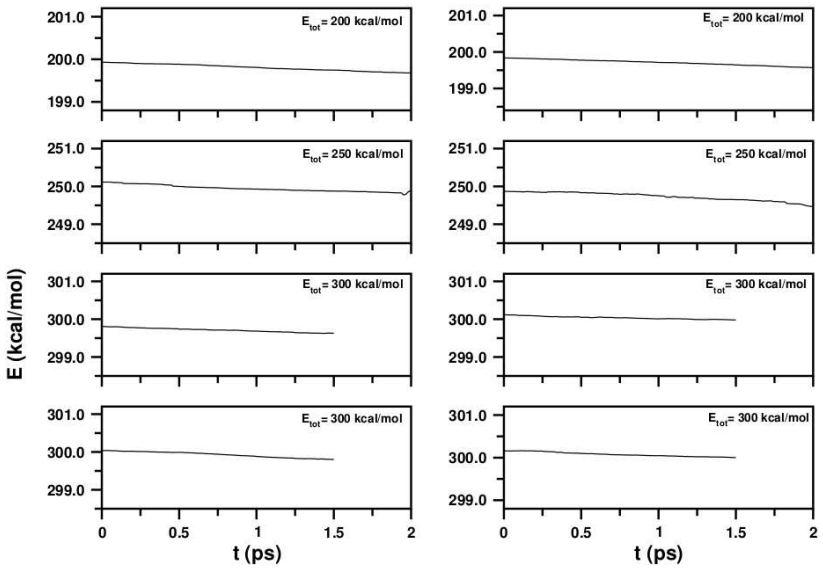

Figure 4.1: Total energy as a function of time for a few sample classical trajectories. In all plots, x-axes ranges are same y-axes show total energy in units of kcal/mol.

decomposition involves formation of a cyclic peroxide isomer (c-$C_3H_6O_3$, -8.9 kcal/mol) via TS1 and the cyclic peroxide dissociates to the CH_3COOH + HCHO or CH_3CHO + HCOOH products via TS2A (29.0 kcal/mol) or TS2B (26.0 kcal/mol), respectively. Reaction coordinates of TS2A and TS2B involve intramolecular proton transfer with concomitant C-C cleavages. Prior to dissociation, the reaction products form product complexes INT2A or INT2B. Korcek decomposition was not observed in the direct dynamics simulations reported below but it is included here for discussion purposes since it was proposed to be an important dissociation pathway of KHP resulting in acids and carbonyl products. TS3 and TS4 are concerted transition states resulting in H_2O + $CH_2(CHO)_2$ (malondialdehyde) and HOOH + CH_2CHCHO (acrolein) products, respectively. Among these two pathways, malondialdehyde channel has the lower energy requirement and is exoergic. Five different

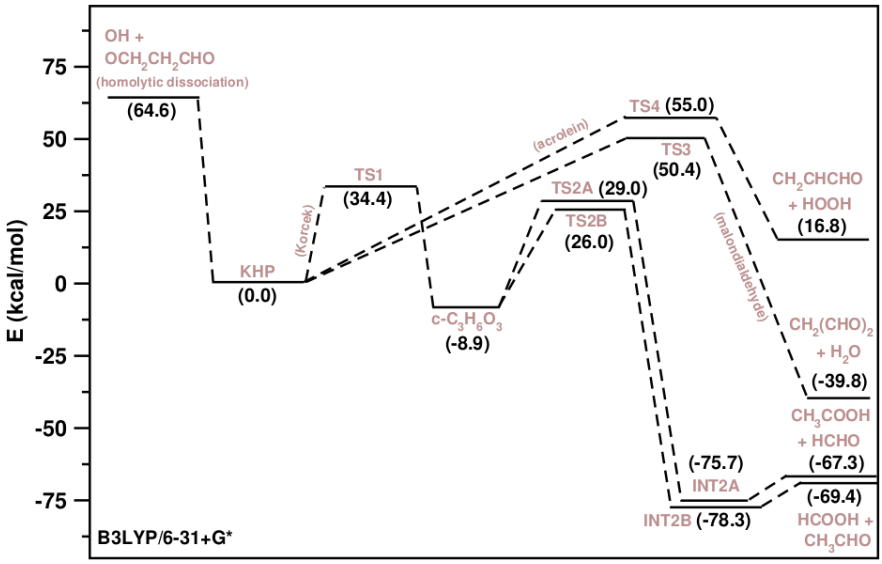

Figure 4.2: Dissociation energy profile of KHP computed using B3LYP/6-31+G* level of electronic structure theory. Energies are given in kcal/mol units and zero point energy not corrected.

mechanisms were found by automated methods[Grambow *et al.*, 2018] for the malondialdehyde channel which included 1,2- and 1,3-H transfer. Here, one of those pathways is reported which was observed in the simulations. Descriptions and optimized geometries of all the stationary points are given in Figure 4.3.

4.2 RESULTS AND DISCUSSION

Simulations were performed at three different total energies and at each E_{tot} (200, 250, and 300 kcal/mol), 200 trajectories were propagated amounting to a total of 600 trajectories. Trajectories were analyzed for reaction pathways and mechanisms. Within the stipulated integration time, 8.5, 55, and 97% of trajectories showed reactivity at E_{tot} = 200, 250, and 300 kcal/mol, respectively. Here reactivity indicates unimolecular dissociation or isomerization before criteria for stopping the trajectory calculations were reached. A variety of reaction products were observed via different unimolecular dissociation pathways and a summary is presented in Table 4.2 which shows classification of the direct dynamics trajectories based on initial dissociation steps. A major fraction of the trajectories dissociated via homolytic dissociations (paths 1, 3, 5, and few minor pathways) in comparison to molecular product formation viz., malondialdehyde [$CH_2(CHO)_2$] (path 2) and acrolein [CH_2CHCHO] (path 4) channels. An important observation is that the Korcek decomposition of KHP was not observed in any of the trajectories. Backbone atoms of KHP were numbered as shown in Figure 4.4 for discussion purposes.

4.2.1 Homolytic Dissociations

Primary homolytic scissions observed in the simulations were that of O(5)-O(6) and C(3)-C(4). Reaction products of these dissociations are OH + HCHO + CH_2CHO (path 1, in Table 4.2). In the present simulations, 7, 52, and 73 trajectories dissociated via this pathway at E_{tot} = 200, 250, and 300 kcal/mol, respectively. Bond dissociation energy (BDE) for O(5)-O(6) dissociation is 64.6 kcal/mol, computed using B3LYP/6-31+G* theory. O(5)-O(6) dissociation leads to OH radical and OCH_2CH_2CHO which undergoes subsequent C(3)-C(4) dissociation resulting in

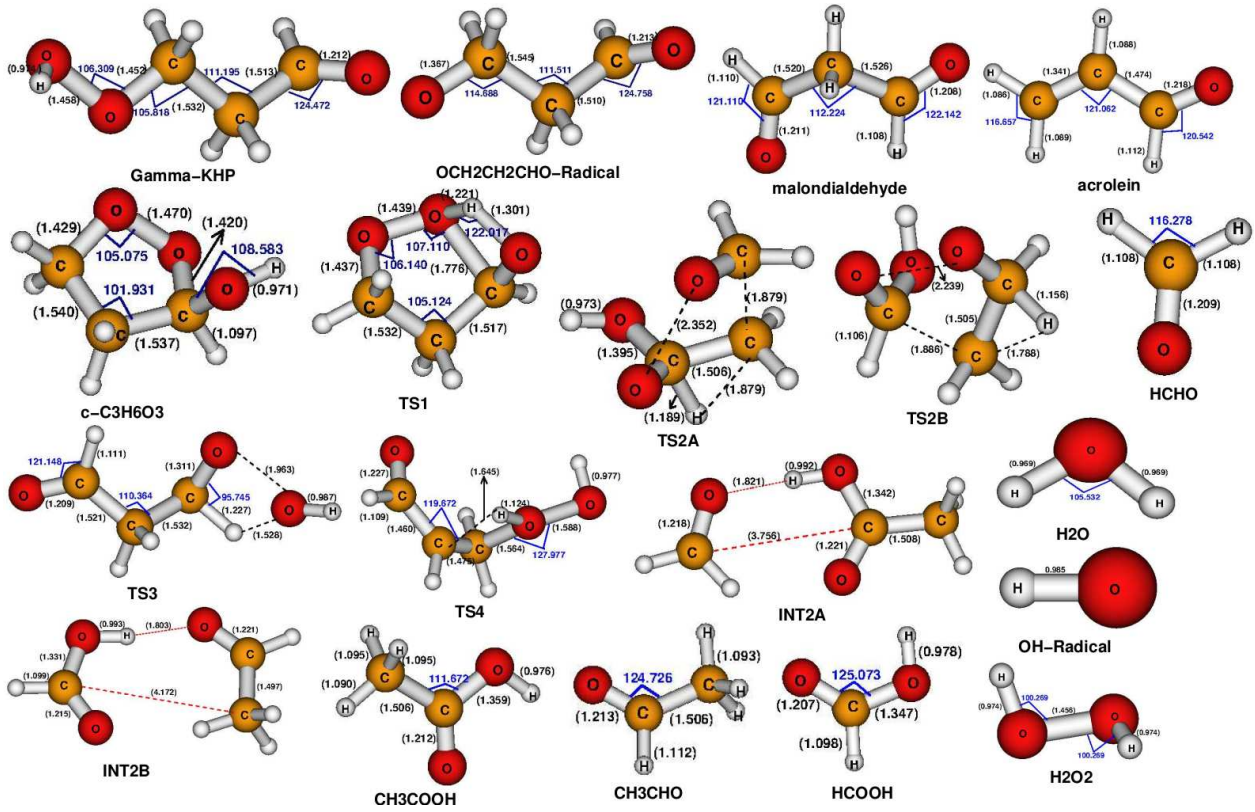

Figure 4.3: Equilibrium geometries of reactant, products, and all the transition states computed using B3LYP/6-31+G* theory.

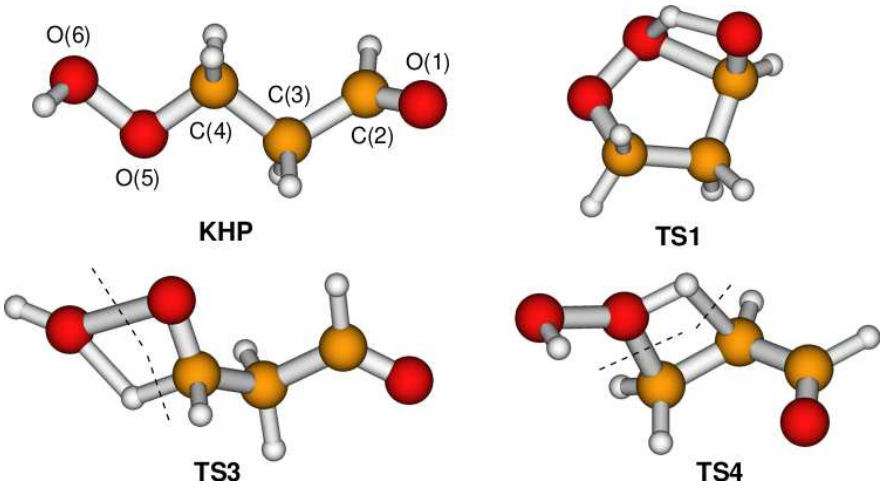

Figure 4.4: Numbering of backbone atoms of KHP used in the text for discussion purposes and the optimized geometries of TS1, TS3, and TS4.

Table 4.2: Number of direct dynamics trajectories classified based on initial dissociation steps.

S.No.	Pathway	200 (kcal/mol)	250 (kcal/mol)	300 (kcal/mol)
1.	OH + HCHO + CH_2CHO (homolytic dissociation, path 1)	7	52	73
2.	H_2O + $CH_2(CHO)_2$ (malondialdehyde channel, path 2)	4	18	39
3.	OOH + CH_2CH_2 + CHO (homolytic dissociation, path 3)	1	9	22
4.	HOOH + CH_2CHCHO (acrolein channel, path 4)	2	9	12
5.	OH + c-C_2H_4O + CHO (homolytic dissociation, path 5)	0	0	5
6.	minor pathways	3	22	43
7.	no reaction	183	90	6
	total	200	200	200

HCHO + CH_2CHO. In addition to OH + HCHO + CH_2CHO, different reaction products were observed following O(5)-O(6) and C(3)-C(4) dissociations. These occur via concomitant proton transfers with the homolytic scissions and subsequent dissociations of the primary products. A summary of observed reaction products is given in Table 4.3 which shows number of trajectories resulting in a particular product following the O(5)-O(6) and C(3)-C(4) dissociations. One important observation from the table is that formaldehyde and acetaldehyde are main products following O(5)-O(6) and C(3)-C(4) dissociations. High yields of carboxylic acid formation during the thermal decay of γ-ketohydroperoxides have been reported[Cord *et al.*, 2012]. Based on electronic structure calculations, Green and coworkers[Jalan *et al.*, 2013] have proposed that Korcek decomposition is a major source of carboxylic acids (HCOOH and CH_3COOH) and carbonyl compounds (HCHO and CH_3CHO) from KHP. Energy profile (B3LYP/6-31+G*) for this pathway is shown in Figure 4.2. In the direct dynamics simulations reported here, none of the trajectories dissociated via the Korcek pathway indicating that this mechanism is not preferred at least under the current simulation conditions. Snapshots of few example trajectories showing O(5)-O(6) and C(3)-C(4) dissociations are shown in Figures 4.5(a) and (b). Numbers inside each frame is time in fs at which the snapshot was taken. In Figure 4.5(a), O(5)-O(6) and C(3)-C(4) cleavages resulting in OH + HCHO + CH_2CHO products can be observed in the 352 fs frame. Figure 4.5(b) shows formation of H_2O + CO + CH_3CHO products. Following C(3)-C(4) dissociation, proton transfer occurs in the 75 fs frame followed by O(5)-O(6) dissociation in the 187 fs frame. Further, another proton transfer from CHO to OH occurs in the 285 fs frame, resulting in the final products.

The second most important homolytic dissociation reaction involved C(4)-O(5) and C(2)-C(3) cleavages resulting in OOH + CH_2CH_2 (ethylene) + CHO products (path 3). In the dynamics simulations, 1, 9, and 22 trajectories dissociated via this pathway at E_{tot} = 200, 250, and 300 kcal/mol, respectively. BDE for C(4)-O(5) bond is 65.4 kcal/mol resulting in OOH + CH_2CH_2CHO which is followed by $CH_2CH_2CHO \rightarrow CH_2CH_2$ + CHO. In a few trajectories, the CHO product dissociated further resulting in CO + H and occasionally H transferred to OOH radical resulting in CH_2CH_2 + CO + HOOH products. In 5 trajectories at E_{tot} = 300 kcal/mol, C(2)-C(3) and O(5)-O(6) dissociations occurred resulting in OH + CHO + OCH_2CH_2. The OCH_2CH_2 cyclized upon formation resulting in cyclic ethylene oxide (c-C_2H_4O) product (shown as path 5 in Table 4.2). Among the cyclic products of KHP dissociation predicted by Grambow and co-workers[Grambow *et al.*, 2018], only ethylene oxide was observed in the present study. Snapshots of example trajectories forming OH + CHO + c-C_2H_4O products are shown in Figure 4.6(b).

Table 4.3: Number of trajectories resulting in various products following O(5)-O(6) and C(3)-C(4) dissociations.

pathway	200 (kcal/mol)	250 (kcal/mol)	300 (kcal/mol)
$CH_2CHO + OH + HCHO$	2	25	20
$CH_2CHO + H_2O + CHO$	0	1	8
$CH_2CHO + CO + OH + H_2$	0	0	1
$CH_3CHO + H_2O + CO$	1	13	10
$CH_3CHO + HO + CHO$	0	3	5
$CH_3CHO + HO + H + CO$	0	0	3
$CH_3CHO + H_2 + CO_2$	0	0	1
$CH_2CO + HCHO + H_2O$	1	5	8
$CH_2CO + HCHO + OH + H$	0	0	5
$CH_2CHOH + H_2O + CO$	3	2	0
$HCHO + CH_2(OH)CHO$	0	0	3
$3HCHO$	0	1	3
$HCHO + CO + OH + CH_3$	0	1	3
$H_2O + 2CO + CH_4$	0	0	1
$HCHO + CH_2OH + CHO$	0	0	1
$HCHO + CH_3COOH$	0	1	1

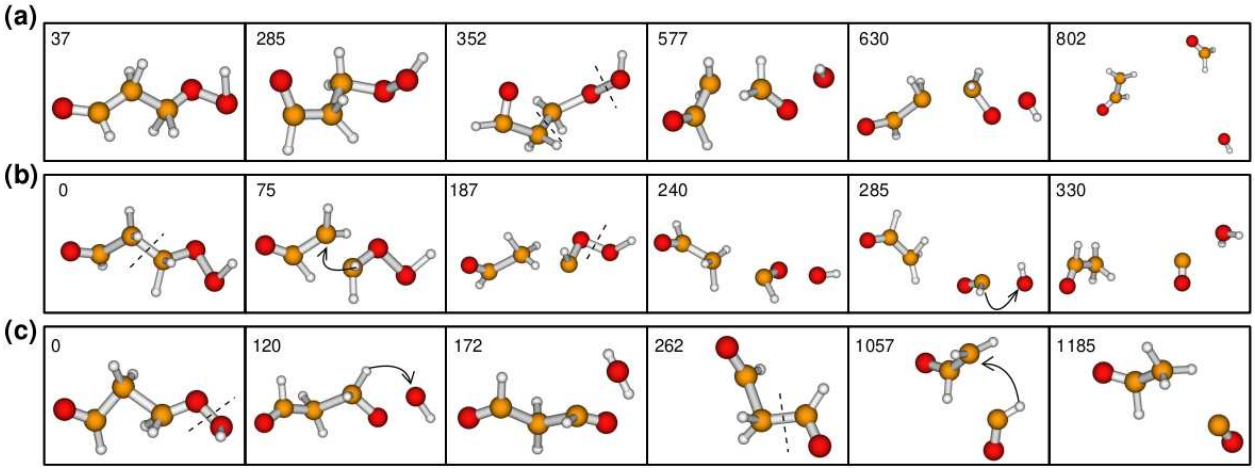

Figure 4.5: Snapshots of example trajectories showing different KHP unimolecular reactions. (a) KHP $\rightarrow$ OH + HCHO + CH_2CHO, (b) KHP $\rightarrow$ H_2O + CO + CH_3CHO, and (c) KHP $\rightarrow$ H_2O + $CH_2(CHO)_2$ $\rightarrow$ H_2O + CO + CH_3CHO. Number inside every frame is time in fs at which the snapshot was taken.

4.2.2 Malondialdehyde Channel

The malondialdehyde channel (path 2, Table 4.2) resulting in H_2O + $CH_2(CHO)_2$ products was observed in an appreciable fraction of trajectories. This is the dominant pathway among the observed molecular product formation channels. As shown in Figure 4.2, this reaction occurs via TS3 with a barrier of 50.4 kcal/mol. The TS3 geometry is shown in Figure 4.4. Overall, the reaction is exoergic with a product energy of -39.8 kcal/mol relative to the reactant. Using automated reaction discovery methods, Suleimanov and co-workers[Grambow *et al.*, 2018] predicted five different routes for the malondialdehyde formation reaction. These include 1,2- and 1,3-H_2O eliminations and roaming of H around O of the CHO group before bonding to another O of the OH group. Energy barriers for these multiple pathways were predicted in the range of 50-70 kcal/mol. In the present work, only the 1,2-H_2O elimination occurring by a proton transfer from C(4) to O(6) with concomitant O(5)-O(6) dissociation was observed. This 1,2-H_2O elimination was predicted to be the lowest energy malondialdehyde pathway in the previous work[Grambow *et al.*, 2018]. Subsequent dissociation of malondialdehyde was also observed which led to CH_2CHO, CH_2CO (ketene), CH_3CHO, HCHO, etc. A summary of these is presented in the Table 4.4. Malondialdehyde channel also led to the formation of aldehydes and carbonyl compounds. Snapshots of an example trajectory forming H_2O + malondialdehyde via 1,2-H_2O elimination are shown in Figure 4.5(c). In the 120 fs frame, the proton transfer with concomitant O-O dissociation can be observed. Subsequent dissociation of malondialdehyde forming CO + CH_3CHO (acetaldehyde) can also be seen in the 1057 fs frame.

Table 4.4: Subsequent dissociation products of malondialdehyde channel.

pathway	200 (kcal/mol)	250 (kcal/mol)	300 (kcal/mol)
H_2O + $CH_2(CHO)_2$	4	15	26
H + OH + $CH_2(CHO)_2$	0	0	4
H_2O + CH_2CHO + CHO	0	0	3
H_2O + CH_2CO + HCHO	0	0	2
H_2O + CH_2CO + H_2 + CO	0	1	0
H_2O + CO + CH_3CHO	0	1	2
H_2O + CO + CH_2CHOH	0	1	2

4.2.3 Acrolein Channel

Path 4 in Table 4.2 corresponds to KHP dissociation to HOOH (hydrogen peroxide) + CH_2CHCHO (acrolein) which was observed in 2, 9, and 12 trajectories at E_{tot} = 200, 250, and 300 kcal/mol, respectively. Energetically, this reaction is less favorable than the malondialdehyde channel but still lower in energy than the homolytic dissociation. Acrolein formation is endoergic with a reaction energy of 16.8 kcal/mol and a barrier height of 55.0 kcal/mol. Reaction mechanism involves transfer of a proton from C(3) to O(5) with simultaneous C(4)-O(5) dissociation. The acrolein pathway was predicted earlier[Grambow *et al.*, 2018] with a barrier height of around 55 kcal/mol and the present calculations indicate a similar barrier for this pathway. In a small number of trajectories, acrolein product resulted via mechanism other than the one discussed here. They are discussed in the next section as minor reaction channels.

4.2.4 Minor Channels

In addition to the fragmentation pathways described above, a number of different products and mechanisms of KHP decomposition were observed in the simulations. These pathways were observed in less than 5 trajectories at a given E_{tot} and are classified as minor dissociation channels.

Table 4.5: Minor dissociation products of KHP unimolecular dissociation.

pathway	yes/no	200 (kcal/mol)	250 (kcal/mol)	300 (kcal/mol)
OOH + CH_2CH_2CHO	no	0	2	2
H + O_2 + CH_2CH_2CHO	no	0	0	1
2OH + CH_2CHCHO (acrolein)	yes (R74)	0	0	1
OOH + H + CH_2CHCHO (acrolein)	yes (R74)	0	0	2
CO_2 + H_2 + CH_3CHO (acetaldehyde)	yes (R14)	0	0	1
CO + H_2O + CH_3CHO (acetaldehyde)	yes (R14)	0	0	1
CHO(OH) + CH_3CHO (acetaldehyde)	yes (R69)	0	4	0
$2H_2O$ + HCCCHO	no	0	0	2
OOH + CO + CH_3CH_2 (ethyl radical)	no	0	0	3
O_2 + CHO + CH_3CH_2 (ethyl radical)	no	0	0	1
CH_2OH + H + $(CHO)_2$ (glyoxal)	no	0	0	1
CH_2OH + HCO + HCHO	no	0	3	0
CH_2OH + HCO + H_2 + CO	no	0	1	0
3HCHO	no	0	1	1
2HCHO + H_2 + CO	no	0	0	2
2HCHO + H + CHO	no	0	0	2
HCHO + OH + CH_3 + CO	no	0	0	2
HCHO + HOOH + HCCH (acetylene)	no	0	0	1
HCHO + O_2 + CH_2CH_2 (ethylene)	yes (R23)	0	0	1
HCHO + CH_2 + CHO(OH) (formic acid)	yes (R69)	0	0	1
HCHO + CO + CH_3OH (methanol)	no	0	0	3
HCHO + H_2 + 2CHO	no	0	0	1
CH_2CO + H_2 + c-CO_2H_2 (dioxirane)	no	0	0	1
CH_2CO + $CH_2(OH)_2$ (methanediol)	yes (R65)	0	0	1
CH_2CO + CHO + OH + H_2	yes (R65)	0	0	1
CH_2CO + HCHO + H_2O	yes (R28)	0	3	0
H_2 + 2CO + CH_3 + OH	no	0	0	2
H_2 + 2CO + CH_2 + H_2O	no	0	0	1
HOOH + CH_2CHCOH	yes (R74)	0	0	1
H_2O + $CH_2(OH)$-C-CHO	no	0	1	1
H_2O + H_2 + CO_2 + HCCH (acetylene)	no	0	0	1
H_2O + H_2 + CH(CO)CHO	no	0	0	1
H_2O + CO + CH_2CHOH (vinyl alcohol)	yes (R17)	0	2	1
OH + CHO + CH_2CHOH (vinyl alcohol)	yes (R17)	0	0	2
CHO(OH) + CH_2CHOH (vinyl alcohol)	yes (R17)	0	2	0
H_2 + CO + CH3COOH (acetic acid)	no	0	0	1
CO + CH_3CH_2OOH	yes (R70)	0	2	0
$HOCH_2OCH_2CHO$	yes (R52)	1	1	0
$HOOCH_2CHCHOH$	yes (R47)	1	0	0
H_2 + $HOOCCH_2CHO$	yes (R12)	1	0	0

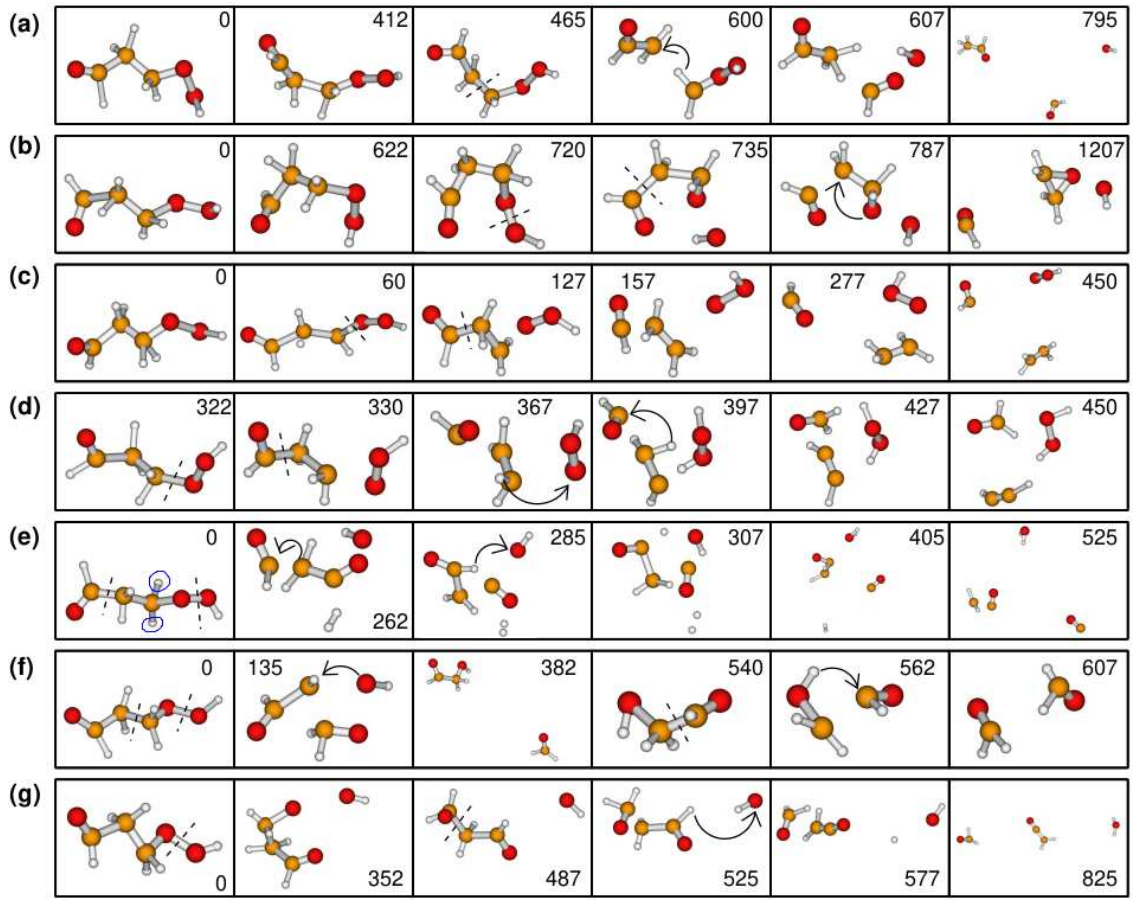

Figure 4.6: Snapshots of example trajectories. The numbers inside each panel is time in fs at which the snapshot was taken. Descriptions of the trajectories are given in the text.

Reaction products of these channels are presented in Table 4.5 along with the number of trajectories showing them. It is also indicated in the table (column 2) that whether the given products were identified in the automated methods reported earlier[Grambow *et al.*, 2018] along with the reaction number used in the previous work. It can be observed from the table that some of the minor dissociation products were predicted in earlier studies and several new dissociation products were also reported. Molecules which are not previously reported as KHP decomposition products and identified in the present work are CH_2CH_2CHO, OOH, CH_3CH_2, CHO, and CH_3 which resulted primarily as homolytic dissociation products. Other molecules such as CH_3CHO (acetaldehyde), HCHO (formaldehyde), HCCH (acetylene), $(CHO)_2$ (glyoxal), CH_2CH_2 (ethylene), CH_2CHCHO (acrolein), CH_3OH (methanol), c-CH_2O_2 (dioxirane), CH_2CHOH (vinyl alcohol), and CH_3COOH (acetic acid) were also observed. Some of these molecules such as CH_3CHO, HCHO, and CH_2CHCHO were also observed in the primary dissociation channels described above. However, the mechanisms were quite different from the primary pathways discussed earlier. For example, the acrolein reported as a minor product did not form via the mechanism involving TS4. The Korcek decomposition products (carboxylic acids and carbonyl compounds) were reported here but the Korcek mechanism was not followed in the simulations. Trajectory snapshots of some minor dissociation channels are presented in the Figure 4.6 and the description of the trajectories is given below.

(a) $HOOCH_2CH_2CHO \rightarrow OH + HCHO + CH_2CHO \rightarrow OH + CHO + CH_3CHO$

(b) $HOOCH_2CH_2CHO \rightarrow OH + OCH_2CH_2 + CHO \rightarrow OH + CHO +$ c-C_2H_4O

(c) $HOOCH_2CH_2CHO \rightarrow OOH + CH_2CH_2 + CHO$

(d) $HOOCH_2CH_2CHO \rightarrow OOH + CH_2CH_2 + CHO \rightarrow HOOH + CHCH_2 + CHO \rightarrow HOOH + HCCH + HCHO$

(e) $HOOCH_2CH_2CHO \rightarrow H_2 + CHO + CH_2CO + OH \rightarrow CH_2CHO + CO + OH + H_2 \rightarrow H_2 + CH_2 + 2CO + H_2O$

(f) $HOOCH_2CH_2CHO \rightarrow OH + HCHO + CH_2CHO \rightarrow HCHO + HOCH_2CHO \rightarrow HCHO + CHO + CH_2OH \rightarrow 3HCHO$

(g) $HOOCH_2CH_2CHO \rightarrow OH + OCH_2CH_2CHO \rightarrow OH + HCHO + CH_2CHO \rightarrow H_2O + HCHO + CH_2CO$

4.3 DISCUSSION

Out of a large number of unimolecular reactions of KHP reported by automated reaction discovery methods, a few are identified as dominant in the current high temperature direct dynamics study. Initial conditions for the trajectories were selected by randomly partitioning the available energy E_{tot} among the vibrational degrees of freedom of the molecule[Peslherbe *et al.*, 1999; Hase and Buckowski, 1980] in the electronic ground state. These sampling conditions mimic reactions occurring in the gas phase. Simulations showed that homolytic scissions were the dominant component of KHP dissociation. The three major dissociation channels viz., homolytic dissociations, malondialdehyde, and acrolein channels were observed in 30.5%, 9%, and 4.5% trajectories, respectively, at $E_{tot} = 250$ kcal/mol; the same fractions were 50%, 19.5%, and 6% in the 300 kcal/mol simulation. With increase in energy (temperature), the overall reactivity of KHP and the fractions of major dissociation pathways increased but no specific energy dependent trends were observed. Also, number of trajectories showing minor dissociation channels increased with energy. Considering the reaction energies and barrier heights, molecular product formation channels such as malondialdehyde and acrolein channels appear to be favorable in comparison to direct dissociations. However, inspection of the geometries of the TSs associated with the molecular channels (shown in Figure 4.4) show the "tightness" of these TSs. Due to such constrained geometrical requirements, homolytic dissociations dominate the unimolecular dissociation of KHP. This point has also been

predicted by Suleimanov and co-workers[Grambow *et al.*, 2018] based on B3LYP calculations. In the present study, the molecular product formation channels involve tight transition states and they are entropically unfavorable[Al Rashidi *et al.*, 2015] over the homolytic dissociations. In a similar manner, the absence of Korcek decomposition of KHP observed in the present study can also be rationalized. Experimental studies[Jensen *et al.*, 1979; Hamilton Jr *et al.*, 1980] have indicated that KHP can be a precursor for carboxylic acids and methyl ketones detected in the chemistry of fuel oxidation and combustion. The Korcek reaction was proposed[Jalan *et al.*, 2013] to be the origin of carbonyl compounds from KHP. As shown in Figure 4.2, Korcek pathway is energetically preferred but the Korcek transition state TS1 is tight and requires a 'bent' position of the molecule i.e., at the TS1, bond formation must occur between C(2) and O(6) and a proton transfer between O(6) and O(1) (Figure 4.4). This process may not occur when sufficient amount of energy is available in the molecule and direct dissociations may be preferred. Korcek pathway can be observed at low energy because it associated with cyclic intermediate. At low energy atoms of KHP molecules spend sufficient time with each other to form cyclic intermediate but in present simulations conditions KHP molecule has enough amount of energy hence atoms of molecule rearrange faster and followed dissocation path. The high yields of carboxylic acids in the thermal decomposition of KHP can be rationalized as follows. The present direct dynamics study shows that carbonyl compounds such as formaldehyde, acetaldehyde, etc. are produced in large quantities during the high temperature decomposition of KHP (Tables 4.2 and 4.3). These compounds upon oxidation under the experimental conditions[Jensen *et al.*, 1979; Hamilton Jr *et al.*, 1980], might be resulting in the observed carboxylic acids.

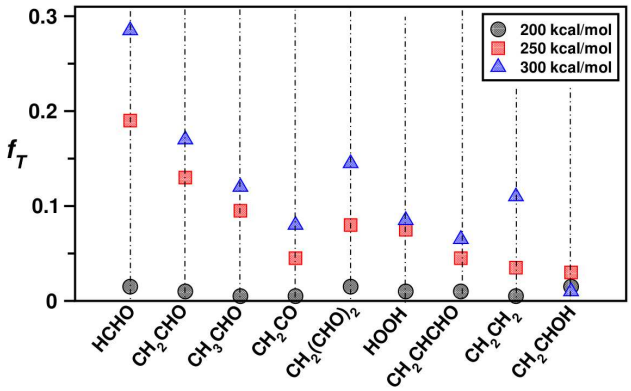

Figure 4.7: Fraction of trajectories f_T resulting in a particular product is shown for various observed reaction products at different total energies E_{tot}.

Figure 4.7 shows the fraction of various reaction products observed in the simulations. The quantity f_T are the ratio between the number of trajectories resulting in a particular species and the total number of trajectories at a given E_{tot}. While computing the fractions, all the trajectories resulting in a particular product, irrespective of the reaction mechanism, were considered. It can be seen from Figure 4.7 that primary dissociation products of KHP are HCHO (formaldehyde), CH_2CHO, CH_3CHO (acetaldehyde), $CH_2(CHO)_2$ (malondialdehyde), and CH_2CH_2 (ethylene). Appreciable quantities of compounds such as CH_2CO (ketene) and HOOH (hydrogen peroxide) are also observed. A few points comparing the present dynamics results with the predictions of previously published[Grambow *et al.*, 2018] automated reaction discovery methods is mentioned here. More than ten reaction channels with cyclic products for KHP decomposition has been predicted. However, the only cyclic product observed in the present study is ethylene oxide c-C_2H_4O in a small number of trajectories (Table 4.2). Five different pathways were predicted earlier for the malondialdehyde + H_2O channel including a roaming mechanism. Out of all these pathways, the lowest energy 1,2-H_2O elimination with the hydrogen transfer occurring from C(4) to O(6) was only observed in the present work irrespective of simulation energy. Isomerization of KHP to different products were predicted but only 2 trajectories in the 200 kcal/mol simulation showed isomerization. Species such as biradicals including carbenes, Criegee intermediates, and zwitterionic structures

which were identified[Suleimanov and Green, 2015; Maeda and Harabuchi, 2019; Grambow *et al.*, 2018] as products of unimolecular reactions of KHP, were either not formed or resulted only as a minor product in a smaller number of trajectories.

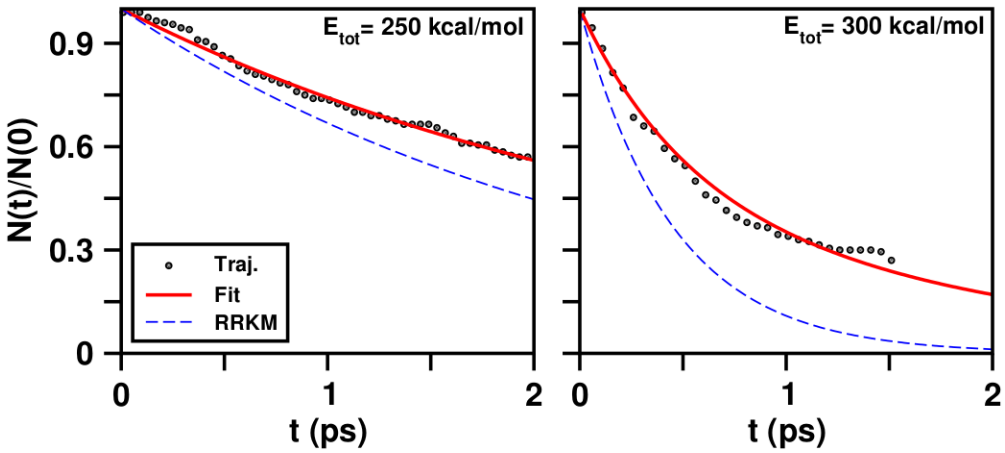

Figure 4.8: Lifetime distributions computed from trajectories and RRKM theory are given as black circles and blue broken lines, respectively. The thick red lines show fit of trajectory data to sum of two exponential functions $N(t)/N(0) = f_1 e^{-k_1 t} + f_2 e^{-k_2 t}$.

To investigate possible non-statistical effects in the dissociation dynamics of KHP, the trajectory lifetime distributions were computed and comparisons were made with predictions from Rice-Ramsperger-Kassel-Marcus (RRKM) theory. From the simulation data, trajectory lifetime distributions[Lourderaj and Hase, 2009] $N(t)/N(0)$ were calculated where $N(t)$ is the number of trajectories that were not reactive at time t and $N(0)$ is the total number of trajectories. The lifetime distribution is a single exponential function $N(t) = N(0)e^{-k(E)t}$ for statistical unimolecular dynamics. Here, $k(E)$ is the RRKM rate constant for an initial microcanonical ensemble[Lourderaj and Hase, 2009]. For non-statistical behavior, trajectory lifetime distribution becomes multi-exponential[Hase *et al.*, 1984] $N(t) = N(0)\sum_i f_i e^{-k_i t}$ where $\sum_i f_i = 1$. Lifetime distributions were calculated from E_{tot} = 250 and 300 kcal/mol simulations and the 200 kcal/mol simulation was not considered because the total number of reactive trajectories was only 17 out of 200. The lifetimes were computed using only those trajectories reacting via pathways 1-4 (Table 4.2) and the minor pathway trajectories were ignored. Classical harmonic RRKM rate constants were computed[Zhu and Hase, 1994] at the simulation energies and were found to be 0.40 and 2.22 ps^{-1} at total energies of 250 and 300 kcal/mol, respectively. The results of these calculations are summarized in Figure 4.8. As can be seen in the figure, the trajectory data deviate from RRKM theory predictions indicating non-statistical nature[Lourderaj and Hase, 2009] of the unimolecular dissociation of KHP. A sum of two exponentials was required to successfully fit the trajectory lifetime distribution data, $N(t)/N(0) = f_1 e^{-k_1 t} + f_2 e^{-k_2 t}$. At E_{tot} = 250 kcal/mol, $f_1 = 0.39, k_1 = 0.47\ ps^{-1}, f_2 = 0.61, k_2 = 0.20\ ps^{-1}$ showing that 40% dissociation occurring in accordance with RRKM predictions and a slow component for the remaining trajectories. Similar behavior was observed at 300 kcal/mol energy also, $f_1 = 0.47, k_1 = 2.09$ ps^{-1}, $f_2 = 0.53, k_2 = 0.59$ ps^{-1}, i.e., a fast and a slow component observed. To investigate the non-statistical dynamics, various coupled phase space models[Paranjothy *et al.*, 2013a] have been proposed but such studies were not performed any further in the present work.

4.4 SUMMARY

Classical chemical dynamics simulations of gas phase unimolecular reaction of γ-ketohydroperoxide are reported. The *on-the-fly* simulations were performed at fixed total energies

using density functional B3LYP method with the 6-31+G* basis set. The results of the simulations were compared with previously reported automated reaction discovery methods. Homolytic scissions were found to be dominant and the Korcek reaction of KHP was not observed in these high energy simulations. Trajectory lifetime distribution calculations showed non-statistical nature of the KHP unimolecular dissociation. In conclusion, the results presented here indicate the need for performing dynamics studies of chemical reactions in order to identify important reaction pathways among the numerous possibilities predicted by automated methods[Suleimanov and Green, 2015; Maeda and Harabuchi, 2019; Grambow *et al.*, 2018].